Available online at www.sciencedirect.com
SCIENCE DIRECT®
International Journal of Heat and Mass Transfer 49 (2006) 3561–3567
International Journal of HEAT and MASS TRANSFER
www.elsevier.com/locate/ijhmt

Effects of droplet size and solute concentration on drying process of polymer solution droplets deposited on homogeneous surfaces

Jun Fukai [a,*], Hirotaka Ishizuka [a], Yosuke Sakai [a], Masayuki Kaneda [a], Masamichi Morita [b], Atsushi Takahara [b,c]

[a] Department of Chemical Engineering, Graduate School of Engineering, Kyushu University, Fukuoka 819-0395, Japan
[b] Department of Chemistry and Biochemistry, Graduate School of Engineering, Kyushu University, Fukuoka 812-8581, Japan
[c] Institute for Materials Chemistry and Engineering, Kyushu University, Fukuoka 812-8581, Japan

Received 21 July 2005; received in revised form 6 February 2006
Available online 19 May 2006

Abstract

An experimental setup is constructed to investigate the drying process of a micro-scale polymer solution droplet deposited on homogeneous surfaces. The contact angle during evaporation does not agree with the contact angle hysteresis measured using an inclined plate method due to the size effect. The average polymer concentration at which the contact line is pinned is independent of the initial solution concentration. This fact reveals that the free convection plays an impotent role before pinning. The pinning time, or the receding distance, is moreover found to be a key factor that dominates the shape and dimensions of the polymer films.

Keywords: Droplet; Evaporation; Drying; Polymer solution; Contact angle; Inkjet printing

1. Introduction

Inkjet printing techniques are lately getting the most attention in the industrial fields regarding electrical, optical and biological devices [1–7]. In these processes, liquid solutions or dispersions deposited as ink on homogeneous or heterogeneous surfaces are dried to form thin films/particle-layers. The drying process of the droplets on the surfaces is accordingly a key technology for controlling the shape of the formed films/particle-layers.

It is well known that a ring structure develops at the periphery of the formed films/particle-layers. Deegan et al. [8] found that the pinning of the contact line plays an important role in the formation of the ring because it causes the radial fluid flow toward the contact line to compensate for the evaporated solvent, resulting in the concentration of the solute. They referred to the pinning of the contact line as *self-pinning*. They also developed a convenient model describing the radial flow and the mass transport, and then numerically demonstrated that the solute is actually concentrated at the periphery of the sessile droplet on substrates [9,10]. Contrary to the use of the droplets on the millimeter diameter order in these studies, Morozumi et al. [11] used polymer solution droplets whose diameters were the same as those in the inkjet printing and discussed the effect of the substrate temperature on the width of the ring stain. As a result, they reported that the model proposed by Deegan et al. [9] predicts the tendency of the experimental results.

The aforementioned studies [8–11] principally focused on the case where the contact line was initially pinned. However, the contact line may be pinned or moved during the initial stage, being dependent on the liquid and surface properties.

As for evaporating pure-liquid droplets on the substrates, Pickness and Bexon [12] observed three distinct evaporation modes: one is the stage that the wetting area remains constant while the contact angle changes, another

* Corresponding author. Tel.: +81 92 802 2744; fax: +81 92 802 2794.
E-mail address: jfukai@chem-eng.kyushu-u.ac.jp (J. Fukai).

0017-9310/$ - see front matter © 2006 Elsevier Ltd. All rights reserved.
doi:10.1016/j.ijheatmasstransfer.2006.02.049

Nomenclature

c_i	initial mass fraction of solute (kg-solute/kg-solution)
c_{av}	average mass fraction of solute (kg-solute/kg-solution)
d_0	initial droplet diameter (m)
d_c	wetting diameter (m)
t	time (s)
Greek symbols	
μ_0	viscosity (kg/m s)
ρ_0	density (kg/m^3)
ψ_c	contact angle of the evaporating droplet (deg)
ψ_A	static advancing contact angle (deg)
ψ_R	static receding contact angle (deg)
$\psi_{c,R}$	receding contact angle of the droplet during evaporation (deg)
ψ_S	static contact angle (deg)

is the inverse case and the other is a mixed mode. Shanahan and Bourges [13] used several sets of liquids and polymer surfaces, and reported that the contact angle at which the contact line starts receding is much lower than the static receding contact angle measured using a classic measurement method. They mentioned that this disagreement is due to the difference between the shear stresses near the contact line. On the other hand, Erbil et al. [14] found disagreement among the contact angles measured by three methods and concluded that these differences are mainly due to the effect of the contact line velocity and the droplet size.

These studies [12–14] used the droplets on the millimeter diameter order, which is much larger than the actual droplets using in inkjet printing. Moreover, the effect of the receding process on the shape of the polymer films is not known in detail.

The purpose of this study is to investigate the effects of the droplet size and the initial concentration during the drying processes of the polymer solution on substrates. The droplets with diameters of 40–100 μm are provided using an inkjet nozzle, while those of the diameters ≈1 mm are done by a syringe. They are referred to as micro-scale and macro-scale, respectively, in this study. The evaporating droplets are photographed using CCD cameras to measure the time histories of their characteristic lengths. The thicknesses of the formed polymer films are measured using laser microscopy. The test surfaces are prepared using a chemical vapor adsorption method. Distilled water is also used as the droplet and compared with the evaporation processes that were previously reported.

2. Experimental

Fig. 1 shows a schematic of the experimental setup used. The inkjet generator is handmade. Micro-scale droplets with diameters less than 100 μm were ejected from a ϕ 50 μm orifice. The diameter of the droplet was controlled by the waveform and voltage applied to the piezo-ceramic actuator placed in the generator. Macro-scale droplets with diameters of about 1 mm were generated from a tip of a needle (0.15-mm inner diameter × 0.72-mm outer diameter) attached to a syringe. The side and top views of the droplets deposited on a substrate were recorded using CCD cameras (30 fps) through zoom lenses (×max. 400). The wetting diameter and droplet height were measured from the pictures. It was verified that the wetting diameters measured from the pictures using the two cameras agreed. The contact angle ψ_c was calculated assuming a spherical droplet cap. The substrate surfaces were controlled at 297 ± 1 K using an isothermal water bath. The experiments were carried out under open atmospheric condition at the temperature 298 ± 1 K and the relative humidity 50 ± 10%.

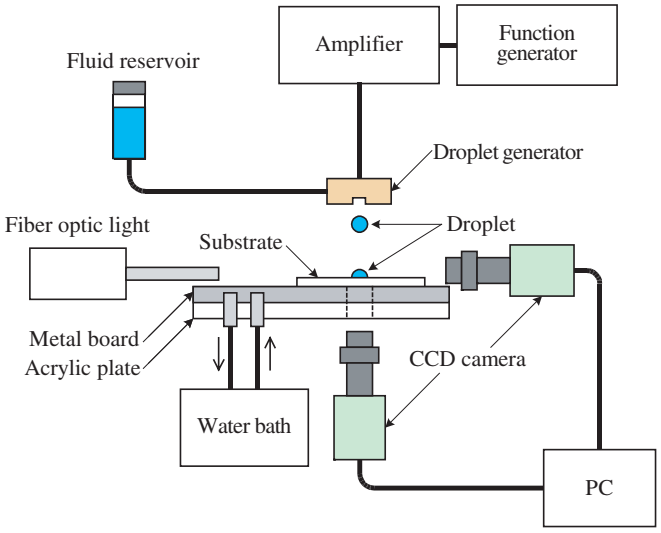

Fig. 1. Schematic diagram of the experimental setup.

Distilled water and a xylene–polystyrene (Acros Organics, average m.w. = 250,000) solution were used as the droplet. The initial solute concentration ranged between 0 and 10.0 wt.%. As test surfaces, a perfluorohexylethyltrimethoxysilane monolayer (R_f) and 3-mercaptopropyltrimethoxysilane monolayer (SO_3H) were coated on silicon wafer plates by a chemical vapor adsorption method [15,16]. Tables 1 and 2 show the contact angles measured using an inclined plane method. These tables show the

Table 1
Static contact angles of distilled water droplet on the SO_3H and R_f surfaces measured by a inclined plane method

Surface	ψ_S (deg)	ψ_R (deg)	ψ_A (deg)
SO_3H	52.8 ± 2.5	31.0 ± 3.9	54.2 ± 0.9
R_f	106.1 ± 0.1	97 ± 1.8	106.5 ± 1.8

Table 2
The static contact angles of xylene–polystyrene droplets on the R_f surface measured by a inclined plane method

c_i (–)	ψ_S (deg)	ψ_R (deg)	ψ_A (deg)
0	68.7 ± 0.5	65.2 ± 0.6	69.8 ± 0.4
0.005	67.0 ± 0.5	64.5 ± 0.3	69.5 ± 0.6
0.030	67.2 ± 0.2	57.9 ± 0.6	69.3 ± 0.1
0.100	63.4 ± 0.6	50.3 ± 0.6	68.7 ± 0.9

average values and the absolute errors of five measurements. The droplet volume was 10 μl. The contact angles of the xylene–PS (polystyrene) droplets on the SO_3H surface are less than 10°. In Table 1, the static receding contact angle ψ_R obviously decreases with increasing c_i. The static contact angle ψ_S, which is the contact angle deposited on a horizontal plate, and the static advancing contact angle ψ_A also tend to decrease with increasing c_i.

The surface tension coefficient measured by the Whilhelmy plate method was almost constant ($28.0–28.3 \times 10^{-3}$ N/m) in the range $c_i = 0–10.0$ wt.%. This fact shows that the dissolved polymer does not restructure on the free surface. On the other hand, the viscosity of the fluid measured by a cone and plate method increased from 0.58×10^{-3} to 16.7×10^{-3} Pa s in the range $c_i = 0–10.0$ wt.%. The force to move a sessile droplet on an inclined plate is proportional to the surface tension coefficient and the difference between cosines of ψ_A and ψ_R [17]. This theory reveals that, in the present system, the force increases with increasing solute concentration. This may be because the polymer strengthens the adhesive forces on the solid–liquid interfaces.

3. Results

Two typical evaporation processes were found as shown in Fig. 2. One is that the wetting diameter d_c remains constant while the contact angle ψ_c decreases. The other is that d_c decreases while ψ_c remains constant.

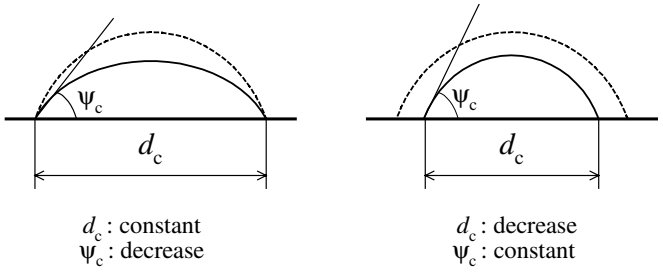

Fig. 2. The definitions of the contact angle and the wetting diameter on the droplet.

3.1. Drying process

3.1.1. Water droplets

Fig. 3 shows the time variations in the contact angle ψ_c and the wetting diameter d_c of the macro-scale water droplets on the SO_3H and R_f surfaces. For the SO_3H surface, d_c remains constant and ψ_c decreases during the initial stage because the contact angle during the spread process is near the advancing contact angle ψ_A, and then reduces to the receding contact angle ψ_R before receding. On the other hand, the constant-d_c stage is very short on the R_f surface because ψ_A is closer to ψ_R on the R_f substrate (Table 1). The results for the micro-scale droplets are shown in Fig. 4. The evaporation processes are similar to those in Fig. 3 though the life times of the droplet are reduced.

The contact angle at which the contact line starts receding is now represented by $\psi_{c,R}$. From the results for the SO_3H surface in Figs. 3 and 4, $\psi_{c,R}$ is 32° for $d_0 = 1.26$ mm and $\psi_{c,R} = 30°$ for $d_0 = 62$ μm, while $\psi_R = 31°$ in Table 1. Several researchers [13] reported that the $\psi_{c,R}$ of the evaporating droplet is much lower than ψ_R on some polymer surfaces. However, there is little difference between $\psi_{c,R}$ and ψ_R on the surfaces used in this study.

3.1.2. Xylene–polystyrene droplets

Although no result for the SO_3H surface is shown in the figure because the droplet height is too low to be measured, the xylene–PS solutions droplets evaporated without any change in the wetting diameter and formed films. That is, the contact line is initially pinned. These processes were independent of the droplet size.

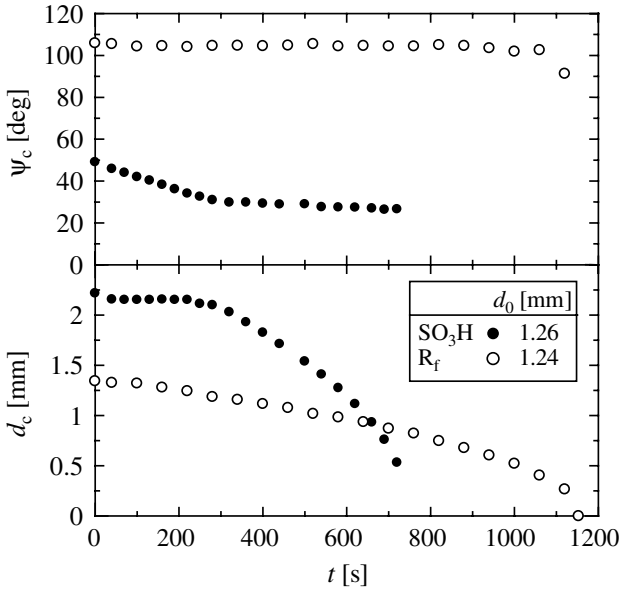

Fig. 3. The time variations in the contact angle and the wetting diameter of the macro-scale water droplets on SO_3H and R_f surfaces.

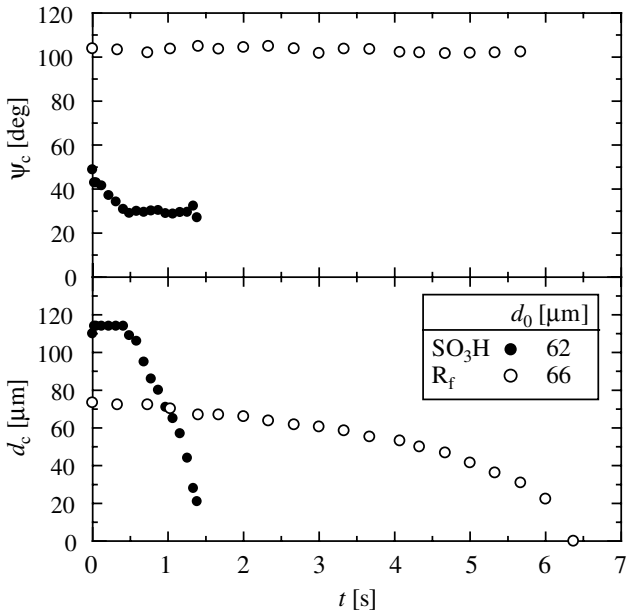

Fig. 4. The time variations in the contact angle and the wetting diameter of the micro-scale water droplets on SO_3H and R_f surfaces.

For the R_f surface, the effect of the initial solute concentration c_i on the evaporating process for the macro-scale droplets is shown in Fig. 5. At the first stage, ψ_c decreases while d_c remains constant. Subsequently, the contact line starts receding while maintaining almost constant contact angle. Moreover, the pinning of the contact line happens at the time when the gradient of the d_c–t curve suddenly changes from a finite value to zero. In these cases, $\psi_{c,R}$ for $c_i = 0$, 0.5 and 3.0 wt.% are about 63°, 55° and 47°, respectively. For $c_i = 0$ wt.%, there is no noticeable difference between $\psi_{c,R}$ and ψ_R (=65.2°) in Table 2. However, $\psi_{c,R}$ obviously decreases as c_i increases. This finding qualitatively agrees with the concentration dependence of ψ_R shown in Table 2 because the solute concentration is elevated due to the evaporation of the solvent. However, a further discussion using such as a numerical simulation is required to estimate the local solute concentration and discuss if they actually agree.

The results for the micro-scale droplets are shown in Fig. 6. The contact line obviously starts receding at a higher contact angle than ψ_R in Table 2. The measured contact angles are known to vary with the droplet size due to the line tension. Good and Kod [18] and Drlich et al. [19] reported that the contact angles decreased with decreasing the droplet diameter. Gaydos and Neumann [20] and Li and Neumann [21] reported the opposite results. Li and Neumann [21] theoretically showed that the droplet-size dependence of the contact angle is determined by the local line curvatures of the contact line, being distorted by the microscopic heterogeneity of the surface. In this study, the diameters of the droplet in the measurement of the contact angles in Table 2 are 2.7 mm because smaller droplets did not move on the incline substrate due to its own weight. Though this size of the droplet is on the same order as the macro-scale droplets in Fig. 5, it is much larger than the micro-scale droplets in Fig. 6. This difference between the droplet sizes is large enough to change the receding contact angles by an order of 10° according to the aforementioned studies [20,21].

To compare the results for the droplets with slightly different diameters, the dimensionless time τ defined as $\mu_0 t/(\rho_0 d_0^2)$ is employed, where μ_0 and ρ_0 are the characteristic viscosity and density, respectively. τ is derived by the

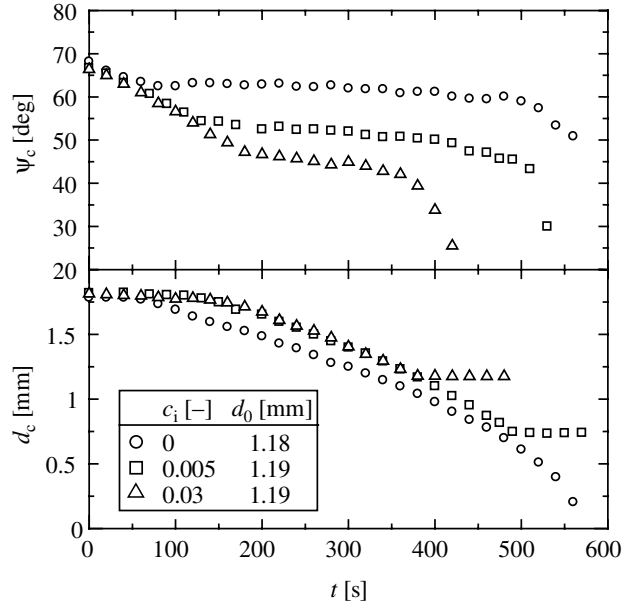

Fig. 5. The time variations in the contact angle and the wetting diameter of macro-scale droplets. The xylene–polystyrene droplets on the R_f surface.

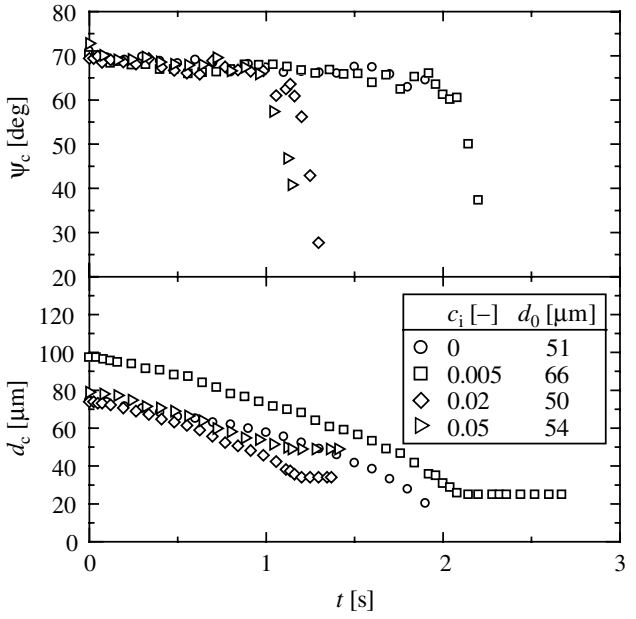

Fig. 6. The time variations in the contact angle and the wetting diameter of micro-scale droplets. The xylene–polystyrene droplets on the R_f surface.

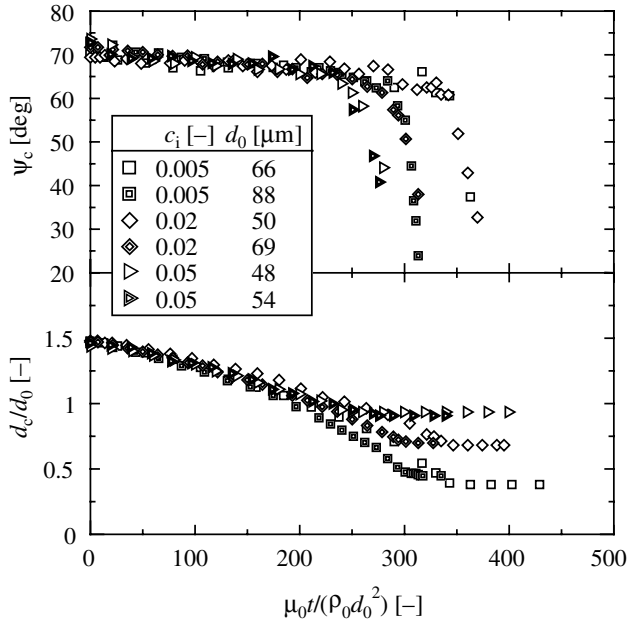

Fig. 7. The variations in the contact angle and the normalized wetting diameter with the dimensionless time. The xylene–polystyrene droplets on R_f surface.

normalization of the Navier–Stokes equations for the free convection [22]. These results are shown in Fig. 7, where d_c is normalized with d_0. The plots for the different initial diameters are almost overlapped for each initial solute concentration, which shows a good reproducibility of the present experiments. This figure also demonstrates that, as the initial concentration increases, the dimensionless pinning time decreases and the shrinkage area of the deposited droplet becomes smaller.

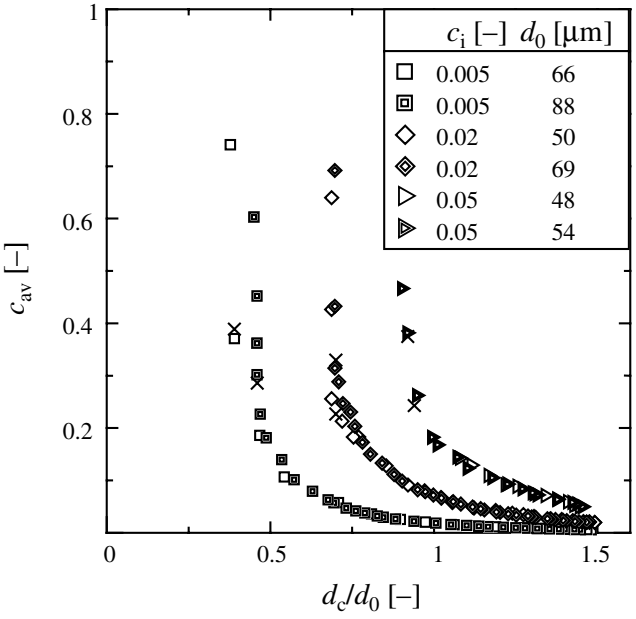

Fig. 8. The average solute concentration during the dry process. The process progresses form the right to the left. The cross indicates where the contact line is pinned.

In Fig. 8, the average solute concentration c_{av} is plotted versus the normalized wetting diameter. The process advances from the right side to the left. The cross indicates where the contact line starts pinning. The pinning is caused in the range $c_{av} = 20$–40 wt.%, being independent of the initial concentration within the experimental error. The contact line is believed to be pinned when the local concentration near the contact line reaches a critical value. c_{av} would strongly depend on the initial concentration if the mass diffusion dominated the mass transfer. Several flow patterns due to Marangoni instability were investigated for the macro-scale evaporating droplets [23,24]. Though those in the micro-scale droplets are not known in detail, a similar free convection must have happened in the micro-scale droplets and played an important role in the mass transport during receding.

3.2. Formed polymer film

Fig. 9 shows a typical profile of a cross section of the formed polymer film for each initial concentration. Though there is a significant difference between the initial concentrations of the droplets, the thicknesses of these films are on the same order due to the fact that lower concentration leads to larger shrinkage of the droplet as shown in Fig. 7.

A dot-like deposit is formed at $c_i = 0.5$ wt.%, while a ring-like one is formed at $c_i = 3.0$ wt.%. The solute must be more uniformly concentrated in the droplet during receding than during pinning because of the free convention in the droplet as already mentioned. The receding process is thus expected to have no significant effect on the difference between the film shapes. The primary reason must be due to the distribution of the evaporation rate on the free surface after pinning. That is, the release of the latent heat on the free surface due to the evaporation results in a temperature gradient on the free surface as well as in the droplet. It is easily expected that the temperature gradient on the free surface decreases with decreasing the size of the evaporating droplet, resulting in a decrease in the gradient of the evaporation rate. As a result, the radial flow toward the contact line, as a cause of the concentration of the solute near the contact line, becomes weak. Morozumi et al. [11] experimentally investigated the relationship between the ring width and the film diameter in the 40 μm–4 mm film diameter range under the condition that the contact line is initially pinned. Although the substrate used by them is different from the present one, the ratio of the width to the diameter tends to increase as the film diameter decreases. This result supports the fact that the phenomena after pinning have an effect on the film shape.

Gans and Schuber [25] demonstrated at an arbitrary condition that the mixture solvent formed a dot-like polymer film while the single solvent formed a ring-like one. They concluded that, for the former case, Marangoni con-

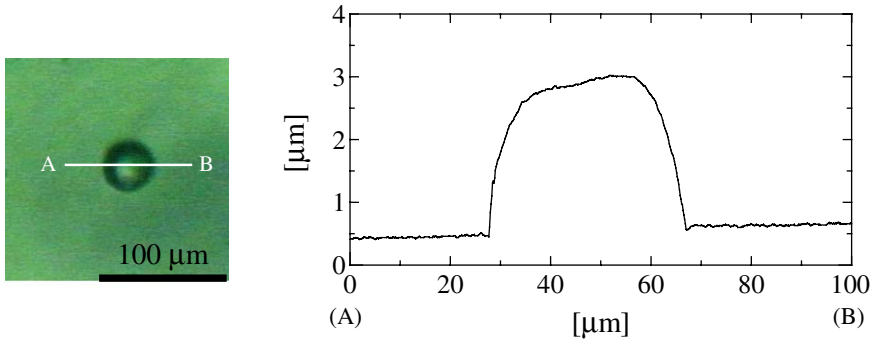

(a) c_i = 0.5 wt. %, d_0 = 98 μm

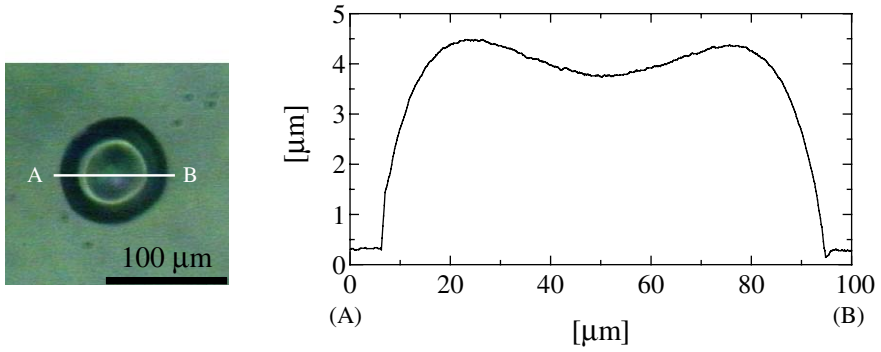

(b) c_i = 3.0 wt. %, d_0 = 100 μm

Fig. 9. Top view and thickness profiles of polymer films.

vection decreases the concentration gradient in the droplet, resulting in the dot-like deposit. This explanation is interpreted as the Marangoni convection delays the pinning time, resulting in larger shrinkage of the wetting area. In fact, the dot-like deposit was smaller in diameter than the ring-like one in their experiment. Considering their work as well as the present one, it is concluded that the pinning time, *or* the receding distance, is the dominant factor that controls the shape and dimensions of the film.

Pauchard and Allain [26,27] used a polymer solution droplet whose initial solute concentration is 20–40 wt.%, and found that the apex height suddenly increases during the drying process, resulting a *Mexican hat*. It is similar to the dot-like deposit in the present study. The *buckling instability* is characterized by a steep increase in the apex height. However, such an increase was not found in the present experiments. The configuration of the films, especially at the film edge, in Fig. 9(a) is moreover different from that of their films. Consequently, the buckling instability is not most likely a principal cause for forming the dot-like deposit.

4. Conclusions

The evaporation/drying processes of water/xylene–polystyrene droplets deposited on substrates were experimentally investigated. The effects of the droplet size and the initial solute concentration on the process were investigated. The significant conclusions are summarized below:

1. For the evaporating water droplet, the contact angles and wetting diameters vary with time according to the contact angle hysteresis measured by a classical method.
2. For the macro-scale xylene–polystyrene droplets, the contact angle at which the contact line starts receding decreases with increasing the initial solute concentration. This tendency of the contact angle agrees with the results measured by a classic method.
3. For the micro-scale xylene–polystyrene droplets, a weak dependence of the initial solute concentration on the drying process is found. The contact line recedes even when the contact angle is above the receding contact angle measured by a classic method.
4. The difference in the process between the macro- and micro-scale xylene–PS droplets is probably due to the size effect.
5. The dot-like and ring-like deposits are formed from the different initial solute concentrations. These films have almost the same thicknesses. This fact shows that the pinning time, or the receding distance, is an important factor to determine the shape and dimensions of the film.

6. The average solute concentration at the pinning is about 20–40 wt.%, within the experimental error, being independent of the initial solute concentration.

Acknowledgements

This research was partially supported by the Japan Society for the Promotion of Science (JSPS), Grant-in-Aid for Science Research (B), no. 16360387.

References

[1] Z. Bao, Y. Feng, A. Dodabalapur, V.R. Raju, A.J. Lovinger, High-performance plastic transistors fabricated by printing techniques, Chem. Mater. 9 (1997) 1299–1301.
[2] S.B. Fuller, E.J. Wilhelm, J.M. Jacobson, Ink-jet printed nanoparticle microelectromechanical systems, J. Microelectromech. Sys. 11 (1) (2002) 54–60.
[3] T. Kawase, T. Shimoda, C. Newsome, H. Sirringhaus, R.H. Friend, Inkjet printing of polymer thin film transistors, Thin Solid Films 438–439 (2003) 279–287.
[4] R. Danzebrink, M.A. Aegerter, Deposition of micropatterned coating using an ink-jet technique, Thin Solid Films 351 (1999) 115–118.
[5] T. Goldmann, J.S. Gonzalez, DNA-printing: utilization of a standard inkjet printer for the transfer of nucleic acids to solid supports, J. Biochem. Biophys. Methods 42 (2000) 105–110.
[6] E.A. Roth, T. Xu, M. Das, C. Gregory, J.J. Hickman, T. Boland, Inkjet printing for high-throughput cell patterning, Biomaterials 25 (2004) 3707–3715.
[7] M. Morita, S. Yasutake, H. Ishizuka, J. Fukai, A. Takahara, Site-selective coating of polymer thin film prepared by the ink-jet method on the patterned fluoroalkylsilane monolayer substrate, Chem. Lett. 34 (7) (2005) 916–917.
[8] R.D. Deegan, O. Bakajin, T.F. Dupont, G. Huber, S.R. Nagel, T.A. Witten, Capillary flow as the cause of ring stains from dried liquid drops, Nature 389 (23) (1997) 827–829.
[9] R.D. Deegan, Pattern formation in drying drops, Phys. Rev. E 61 (1) (2000) 475–485.
[10] R.D. Deegan, O. Bakajin, T.F. Dupont, G. Huber, S.R. Nagel, T.A. Witten, Contact line deposits in an evaporating drop, Phys. Rev. E 62 (1) (2000) 756–765.
[11] Y. Morozumi, H. Ishizuka, J. Fukai, Solute deposit during evaporation of a sessile binary liquid micro-droplet on a substrate, J. Chem. Eng. Jpn. 37 (6) (2004) 778–784.
[12] R.G. Picknett, R. Bexon, The evaporation of sessile or pendant drops in still air, J. Colloid Interface Sci. 61 (2) (1977) 336–350.
[13] M.E.R. Shanahan, C. Bourges, Effects of evaporation on contact angles on polymer surfaces, Int. J. Adhes. Adhes. 14 (3) (1994) 201–205.
[14] H.Y. Erbil, G. McHale, S.M. Rowan, M.I. Newton, Determination of the receding contact angle of sessile drops on polymer surfaces by evaporation, Langmuir 15 (1999) 7373–7385.
[15] T. Koga, M. Morita, H. Ishida, H. Yakabe, S. Sasaki, O. Sakata, H. Otsuka, A. Takahara, Dependence of the molecular aggregation state of octadecylsiloxane monolayers on preparation methods, Langmuir 21 (2005) 905–910.
[16] M. Morita, T. Koga, H. Otsuka, A. Takahara, Macroscopic-wetting anisotropy on the line-patterned surface of fluoroalkylsilane monolayers, Langmuir 21 (2005) 911–918.
[17] M.K. Chaudhury, G.M. Whitesides, How to make water run uphill, Science 256 (1992) 1539–1541.
[18] R.J. Good, M.N. Koo, The effect of drop size on contact angle, J. Colloid Interface Sci. 71 (2) (1979) 283–292.
[19] J. Drelich, J.L. Wilbur, J.D. Miller, G.M. Whitesides, Contact angles for liquid drops at a model heterogeneous surface consisting of alternating and parallel hydrophobic/hydrophilic strips, Langmuir 12 (1996) 1913–1922.
[20] J. Gaydos, A.W. Neumann, The dependence of contact angles on drop size and line tension, J. Colloid Interface Sci. 120 (1) (1987) 76–86.
[21] D. Li, A.W. Neumann, Determination of line tension from the drop size dependence of contact angles, Colloids Surf. 43 (1990) 195–206.
[22] R.B. Bird, W.E. Stewart, E.N. Lightfoot, Transport Phenomena, Wiley, 1960, pp. 310–351.
[23] N.P. Cheremisinoff, Handbook of Heat and Mass Transfer, Gulf Publishing Company, Houston, 1986, pp. 211–229.
[24] R. Savino, D. Paterna, N. Favaloro, Buoyancy and marangoni effects in an evaporating drop, J. Thermophys. Heat Transfer 16 (4) (2002) 562–574.
[25] B.J. De Gans, U.S. Schubert, Inkjet printing of well-defined polymer dots and arrays, Langmuir 20 (2004) 7789–7793.
[26] L. Pauchard, C. Allain, Buckling instability induced by polymer solution drying, Europhys. Lett. 62 (6) (2003) 897–903.
[27] L. Pauchard, C. Allain, Stable and unstable surface evolution during the drying of a polymer solution drop, Phys. Rev. E 68 (2003) 052801.